Int. J. Nano Dimens., 14 (1): 50-59, Winter 2023

ORIGINAL ARTICLE

Innovative fabrication of Ceo$_2$ nanoparticles/WO$_3$ nanoplates S-Scheme heterojunction for visible light photocatalytic degradation of nitenpyram insecticide

Ghader Hosseinzadeh *

Department of Chemical Engineering, University of Bonab, Bonab, Iran

Received31 July 2022; revised 01 September 2022; accepted 12 September 2022; available online 18 September 2022

Abstract

In the current study, a novel S-scheme heterojunction photocatalyst was fabricated through a simple hydrothermal method from CeO_2 nanoparticles and WO_3 nanoplates in presence of tragacanth mucilage as natural surfactant. The prepared heterojunction photocatalyst was used for degradation of Nitenpyram insecticide under visible light irradiation. The successful synthesis of the heterojunction samples was confirmed by FESEM, XRD, PL, DRS, and Mott-Schottky analysis. The results showed that, the photocatalytic performance of the CeO_2/WO_3 heterojunction sample was higher than that of the pure WO_3 and CeO_2 samples. The highest photocatalytic activity was obtained for the sample with 30 wt% CeO_2 content, which has the reaction rate constant of 0.017 min^{-1}. The improved photocatalytic activity of the nanocomposite sample could be related to the efficient separation of the photoinduced electron-hole pairs at the interfaces of WO_3 and CeO_2, and enhanced visible light harvesting. Furthermore, according to the active species trapping tests and Mott-Schottky measurements, hydroxide radical was determined as the main active species for degradation of Nitenpyram insecticide, and a S-scheme charge transfer mechanism revealed to be responsible for the enhanced photocatalytic performance.

Keywords: *CeO_2; Heterojunction; Nitenpyram; S-Scheme; WO_3.*

How to cite this article

Hosseinzadeh G.h. Innovative fabrication of Ceo$_2$ nanoparticles/WO$_3$ nanoplates S-Scheme heterojunction for visible light photocatalytic degradation of nitenpyram insecticide. Int. J. Nano Dimens., 2023; 14(1): 50-59.

INTRODUCTION

Nowadays, various insecticides are widely used in agriculture for the protection of crops from pests. Excessive use of insecticides can lead to the contamination of environmental resources such as groundwater, rivers and soil [1]. Nitenpyram, is one of the most effective neonicotinoid and commonly used in agriculture [2]. Biodegradation, membrane reactors, hybrid adsorption/coagulation/flocculation, catalytic hydrolysis and advanced oxidation process (AOP) are recently developed techniques for elimination of insecticides from the contaminated water [3-7]. Among these techniques, AOP by using semiconductor photocatalysts is a most effective one which widely used in environmental remediation applications [8, 9].

In the recent decades, Tungsten oxide (WO_3), as an n-type semiconductor with a suitable band gap energy of ~2.5 eV for visible light absorption[10], has gained much consideration in the photocatalytic processes due to its interesting features such as suitable valence and conduction band position, high visible light absorption, good stability, low cost, outstanding electrochemical and optical properties [11-14]. However, because of its narrow band gap, fast recombination of the photoinduced electron-hole pairs, and low sunlight harvesting ability, the photocatalytic performance of bare WO_3 is rather low [15]. Based on the above considerations, various methods have been developed to overcome the restrictions of WO_3 such as, doping with metal or nonmetal elements [16, 17], compositing with graphene or g-C_3N_4 [18, 19], engineering of its morphology and surface

* Corresponding Author Email: *g.hosseinzadeh@ubonab.ac.ir*

structure [20, 21], and heterojunction formation with other semiconductors [21, 22]. Currently, as a promising approach, combination of a semiconductor with a second semiconductor in the form of heterojunction photocatalyst has attracted much attention, which leads to the efficient separation of the photoinduced electron-hole pairs and improving of the sunlight absorbance efficiency [23-26].

In the recent decades, CeO_2 have attracted considerable interest in photocatalytic water remediation and environmental applications because of its intrinsic unique properties such as rigid skeleton, very high chemical and photochemical stability, unique fluorite-type structure, non-toxicity, its excellent redox characteristics, and intrinsic oxygen vacancy defects by flexible conversion among cerium's tetravalent and trivalent valence states [22]. However, bare has not remarkable photocatalytic performance. In this regards various strategies have been developed for improvement of its photocatalytic efficiency, including compositing with carbon nanostructures [27, 28], doping with other elements [27, 29], surface engineering [30], and hybridization with other semiconductor photocatalysts in heterojunction nanocomposites [30]. Among these methods, the heterojunction photocatalysts are promising and different heterojunction nanocomposites were synthesized such as form with other semiconductors such as ZnO/CeO_2 [30], Bi_2O_3/CeO_2 [31], $CeO_2/ZnIn_2S_4$ [32], $CeO_2/BiOI$ [33], and $CeO_2/g\text{-}C_3N_4$ [34].

Inspired from the above discussions, in current study, a WO_3-CeO_2 heterojunction nanocomposite was synthesized from new method and with novel morphology by compositing of CeO_2 nanoparticles, and WO_3 nanoplates through hydrothermal technique and was applied for photocatalytic degradation of Nitenpyram insecticide under visible light irradiation. The as-prepared composite was fully characterized by XRD, FESEM, DRS, PL, and Mott-Schottky analysis. Furthermore, based on the optical, photoelectrochemical and photocatalytic activity tests results, a possible charge transfer mechanism was proposed. The major novelties of the current study are preparation of the WO_3-CeO_2 heterojunction with new morphology and via an innovative hydrothermal technique by using tragacanth mucilage as natural surfactant, application of this heterojunction nanocomposite as visible light photocatalyst for degradation of Nitenpyram insecticide, and investigation of the degradation mechanism.

EXPERIMENTAL

Materials

Cerium nitrate hexahydrate, ammonia solution (25 wt%), HCl, ethanol, $Na_2WO_4.2H_2O$, NH_4NO_3 were purchased in analytical grade from Merck, Germany, and were used as raw materials without any purification.

Tragacanth mucilage was prepared by ultrasonic dispersing of 1 g tragacanth gum in 100 ml water at room temperature and stirring for 12 h. The homogenous mucilage was kept at 4 °C.

Synthesis of CeO_2 nanoparticles

CeO_2 nanoparticles were prepared by hydrothermal method. Briefly, 0.5 g of cerium nitrate hexahydrate was dissolved in 50 mL deionized water, then under sonication, ammonia solution (25 wt%) was added in dropwise manner until pH reached to 9. The final suspension was poured into a 75 ml Teflon lined stainless autoclave and maintained at 150 °C for 12 h. The final precipitate were collected by centrifuging, washed several times with deionized ethanol and water, and dried in a vacuum oven at 60 °C.

Synthesis of WO_3 nanoplates

WO_3 nanoplates were also prepared by hydrothermal method. For this purpose, 1 g of sodium tungstate dihydrate ($Na_2WO_4.2H_2O$) was dispersed in 50 ml deionized water, under ultrasonication HCl solution (4 M) was added to above suspension until pH = 1 to complete the solvation of the tungstate salt. After addition of 1g ammonium nitrate (NH_4NO_3) solution, the final solution was transferred into a 75 mL Teflon lined stainless autoclave and maintained at 180°C for 10h. The final precipitates were immediately separated-out by centrifugation, washed several times with distilled water and ethanol, and dried at 60 °C.

Synthesis of WO_3-CeO_2 nanocomposite

In a typical process, for synthesis of WO_3-CeO_2 nanocomposite, containing different weight percentage of CeO_2, 0.5 g of the prepared WO_3 nanoplates were fully dispersed in 45 mL deionized water by probe ultrasonication in presence of 5 ml tragacanth mucilage solution as natural surfactant, then desired amount of cerium nitrate hexahydrate

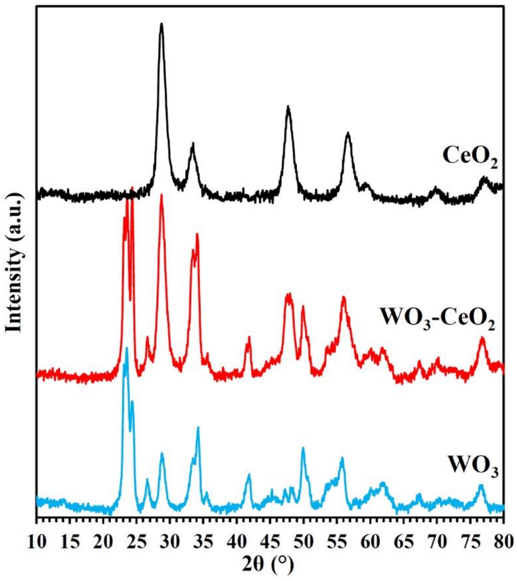

Fig. 1. XRD patterns of the prepared samples.

was dissolved in the above suspension by magnetic stirring. After adjusting of pH at 9 by ammonia solution, the final suspension was poured into a Teflon lined stainless autoclave and maintained at 180°C for 10h. The resulted nanocomposite were separated-out by centrifugation, washed several times with distilled water and ethanol, and dried at 60 °C.

Characterizations

The crystal characteristics of the obtained photocatalysts were analyzed by X-ray diffraction (XRD) on Philips X' Pert MPD with Cu Kα radiation (λ= 0.15406 nm) in 2θ range from 10° to 80°. MIRA3 TESCAN field emission scanning electron microscopy (FESEM) was applied to investigate the morphology and particle size of the photocatalyst samples. Diffuse reflectance spectroscopy (DRS) in the region of 200 to 800 nm was performed by means of a Shimadzu UV-2550 UV–vis spectrophotometer. Varian Cary-Eclipse 500 fluorescence spectrometer was used to obtain the photoluminescence (PL) spectra of samples at excitation wavelength of 300 nm. Photo-electrochemical characteristics of the samples were assessed using a Gamry potentiostat in a conventional three electrode system of Pt foil (counter electrode), Ag/AgCl (reference electrode), and the prepared samples as working electrode under 570 W Xenon lamp equipped with L41 UV-cut off filter (Kenko Co.) irradiation.

Photocatalytic activity

The photocatalytic efficiencies of the synthesized samples were investigated by measuring degradation of Nitenpyram insecticide under visible light irradiation. A 570W Xenon lamp equipped with L41 UV-cut off filter (Kenko Co.) was used as visible light source. Briefly, 30 mg of photocatalyst sample was fully dispersed in 100 mL of the aqueous solution of Nitenpyram. The resulted suspension was maintained under dark condition and stirred for 1 h to reach an adsorption–desorption equilibrium, and afterward was irradiated. Every 20 min, 5 mL of aliquot was sampled and immediately centrifuged to deposit the remnant photocatalyst nanocomposites, and the remaining concentration of Nitenpyram insecticide was measured Cary 100 Bio UV–Vis spectrophotometer.

RESULTS AND DISCUSSION

XRD Analysis

The XRD patterns of the prepared samples were illustrated in Fig. 1. For CeO_2 nanoparticles, the main peaks at 2θ of 28.7°, 33.3°, 47.8°, 56.8°, 59.6°, 69.6°, and 76.6° are respectively assigned to the (111), (200), (220), (311), (222), (400), and (331) crystal planes of CeO_2 with the cubic fluorite structure (JCPDS 01–0800) [35]. In XRD pattern of WO_3, the diffraction peaks positioned at 2θ of 24.3°, 23.3°, 23.5°, 34.3°, 33.4°, 49.8°, and 33.5° can be respectively indexed to the (200), (002), (020),

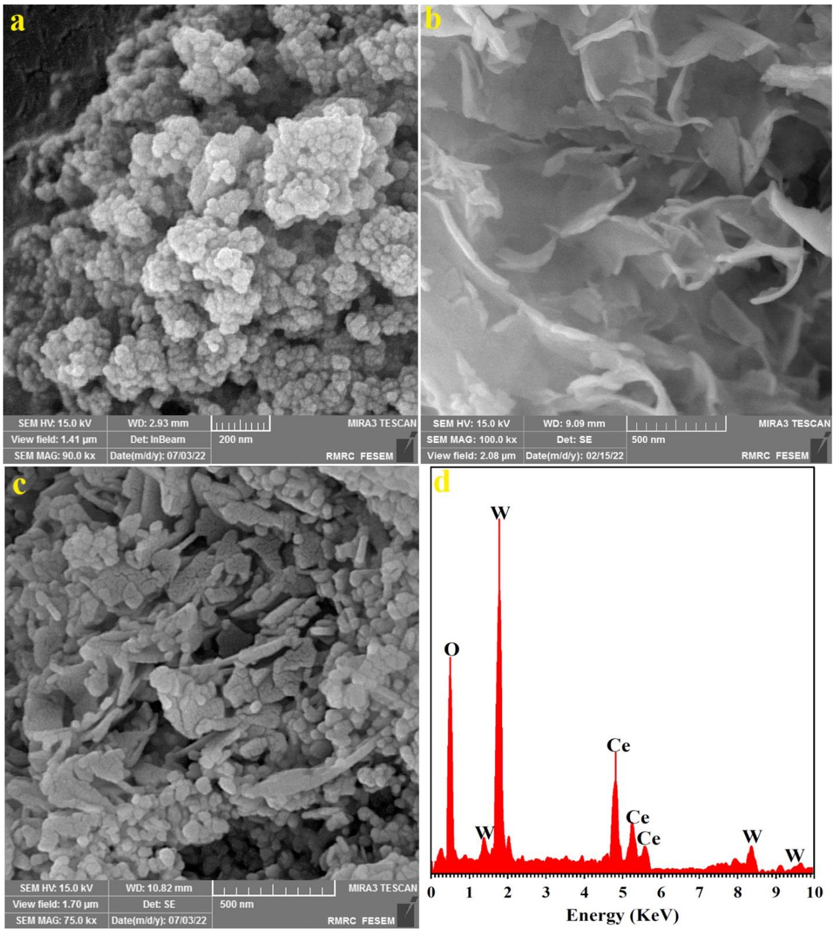

Fig. 2. FE-SEM images of CeO_2 (a); WO_3 (b) and WO_3-CeO_2 heterojunction nanocomposite (c), EDS spectrum of WO_3-CeO_2 heterojunction nanocomposite (d).

(202), (022), (400), and (202) lattice planes of the monoclinic WO_3 phase with JCPDS #83-0951 [36]. In the XRD patterns of WO_3-CeO_2 sample, the characteristic diffraction peaks of both WO_3 and CeO_2 are present, denoting that the nanocomposite sample are successfully synthesized. The broadening of the diffraction peaks indicates nanostructure nature of the prepared samples. The crystallite size of the samples was estimated through the Debye-Scherrer formula [37] as given in equation (Eq. (1)):

$$D = \frac{K.\lambda}{\beta.cos\theta} \qquad \text{Eq. (1)}$$

where K is the Scherrer constant (0.89), D is the crystallite size, θ is the diffraction angle at maximum intensity, λ is the X-ray wavelength, and β is the Full Width at Half Maximum. Based on this calculation, the crystallite size of the WO_3, CeO_2 and WO_3-CeO_2 samples was found to be 12 nm, 17 nm and 20 nm, respectively.

FE-SEM

The FE-SEM images were taken from the WO_3, CeO_2, and WO_3-CeO_2 samples to characterize their morphology and particle size. The results of FE-SEM images for the samples prepared are given in Fig. 2. Fig. 2a demonstrates FE-SEM image of the CeO_2 sample, as seen, this sample contains the CeO_2 nanoparticles with an approximate size of 20-40 nm. Based on the FE-SEM image of the WO_3 sample (Fig. 2b), this sample is made up of WO_3 nanoplates with a thickness of approximately 20 nm. In FE-SEM image of the WO_3-CeO_2 nanocomposite (Fig. 2c), both of the CeO_2 nanoparticles and the WO_3 nanoplates are clearly furthermore, the suitable distribution of the CeO_2 nanoparticles on the WO_3 nanoplates are clearly observed in this image.

To verify the presence of WO_3, and CeO_2 semiconductors in the WO_3-CeO_2 heterojunction

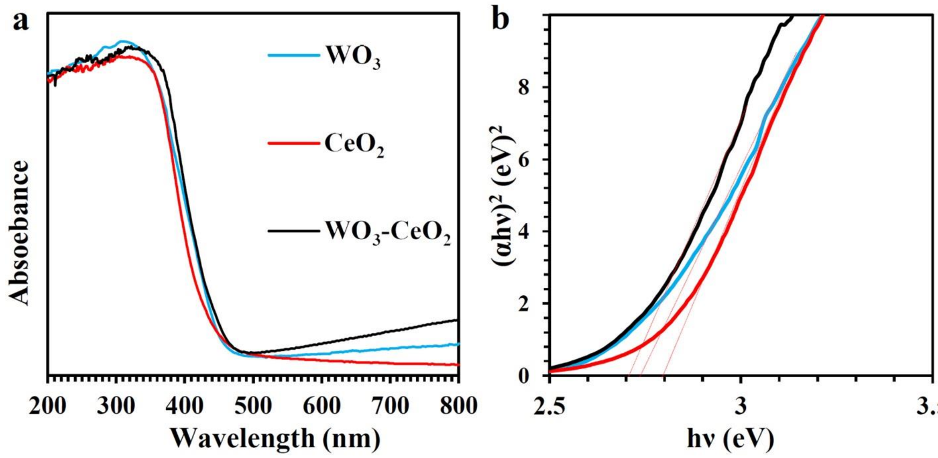

Fig. 3. (a) UV-Vis diffuse reflectance spectra and, (b) Tauc plots for the corresponding samples.

nanocomposite, EDS analysis were carried out on this sample. Fig. 2d shows the EDS spectrum of the WO_3-CeO_2 sample. In the EDS spectrum, peaks corresponding to W, O and Ce can be obviously observed, suggesting the coexistence of WO_3, and CeO_2 semiconductors in the WO_3-CeO_2 sample, which demonstrates successfully synthesis of deposited on the WO_3-CeO_2 heterojunction nanocomposite.

DRS

In order to evaluate the photocatalytic performance of a photocatalyst, its optical behavior must be examined. To study the photo-response characteristics of the prepared samples, the light absorption spectra of the prepared samples were tested by UV-Vis diffuse reflectance spectroscopy (UV-DRS), and the relevant results are shown in Fig. 3. As it is clearly seen in Fig. 3a, the absorption edges of the WO_3, CeO_2, and WO_3-CeO_2 samples are found to be around 460, 395, and 420 nm, respectively. As can be seen, CeO_2 nanoparticles mainly absorb the ultraviolet light. WO_3, on the other hand, has a tendency to absorb visible light radiation. The presence of CeO_2 in the structure of WO_3 shifts the absorption edge of WO_3 towards the visible light range, which can improve the photocatalytic performance of the nanocomposite sample under visible light radiation. In order to study this effect more precisely, the band gap energy of the samples was examined based on Tauc formula [38]. As shown in (Fig. 3b) the band gap energies of the WO_3, CeO_2, and WO_3-CeO_2 samples are 2.74, 2.8, and 2.7 eV, respectively. Therefore, formation of the heterojunction interface between CeO_2 and WO_3 remarkably decreases the band

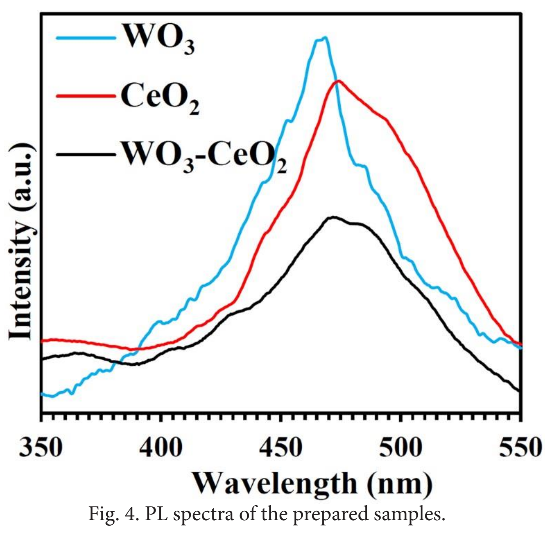

Fig. 4. PL spectra of the prepared samples.

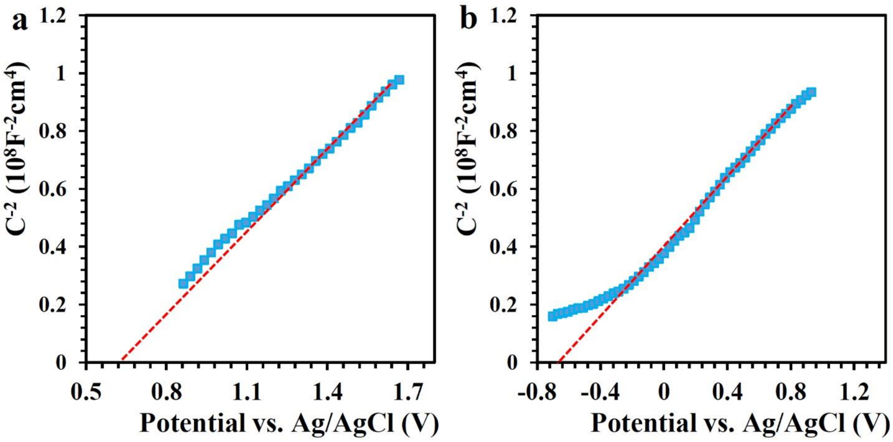

Fig. 5. Mott-Schottky measurements for (a) WO_3 and (b) CeO_2 samples.

gap energy of WO_3, which could results in an improvement of photocatalytic activity under visible light irradiation.

Photoluminescence (PL)

The separation of charge carriers, i.e. photoinduced electrons and holes, is one of the effective factors on the photocatalytic performance of a photocatalyst sample (PL) spectroscopy can be used to study the effect heterojunction formation between CeO_2 and WO_3 semiconductors on the separation and transportation of charge carriers in the WO_3-CeO_2 heterojunction sample. In this case, any decrease in the PL intensity indicates a decrease in the electron-hole recombination which can results in the improvement of the photocatalyst performance [39]. As can be seen in Fig. 4, the PL intensity of the WO_3-CeO_2 nanocomposite is remarkably lower than that of the CeO_2 and WO_3 samples, so it can be concluded that heterojunction formation between CeO_2 and WO_3 effectively reduced the electron-hole recombination. Therefore, the WO_3-CeO_2 sample could have the improved photocatalytic activity due to the diminished charge carriers' recombination rate.

Mott-Schottky

To determine the conduction and valance band energies of the CeO_2, WO_3 samples, Mott-Schottky tests were conducted, as depicted in (Fig. 5). The Mott-Schottky curves of CeO_2 and WO_3 samples have positive slopes, reflecting that these samples are n-type semiconductors [40, 41]. The flat band potentials (E_{FB}) for pure WO_3 and CeO_2 were found to be +0.7 V (Fig. 5a) and -0.64 V (Fig. 5b) versus Ag/AgCl reference electrode (+0.9 V and -0.44 V relative to NHE), respectively. It is generally documented that the conduction band potential (E_C) in n-type semiconductors is located ~0.1 eV lower than E_{FB}, and the potential of valance band (E_V) of p-type semiconductors is approximately 0.1 V higher than E_{FB} [40]. In this regard, E_C of CeO_2

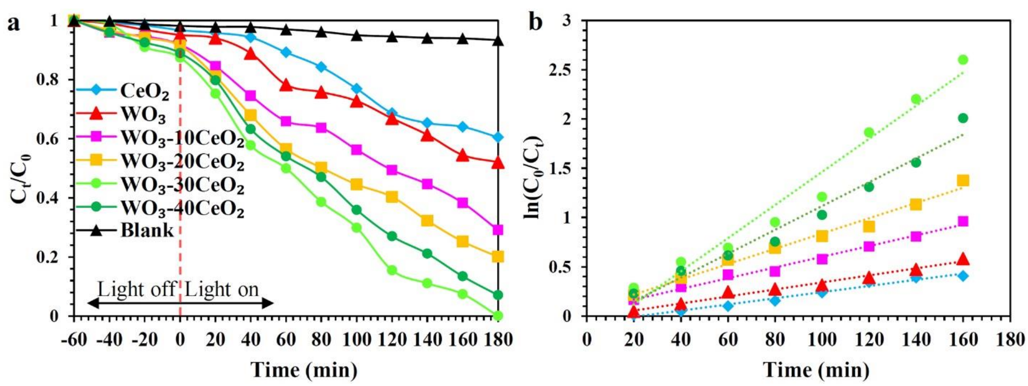

Fig. 6. (a) Visible light photocatalytic treatment of Nitenpyram insecticide over the prepared samples, and (b) Pseudo first-order reaction kinetics for Nitenpyram degradation over the prepared photocatalysts.

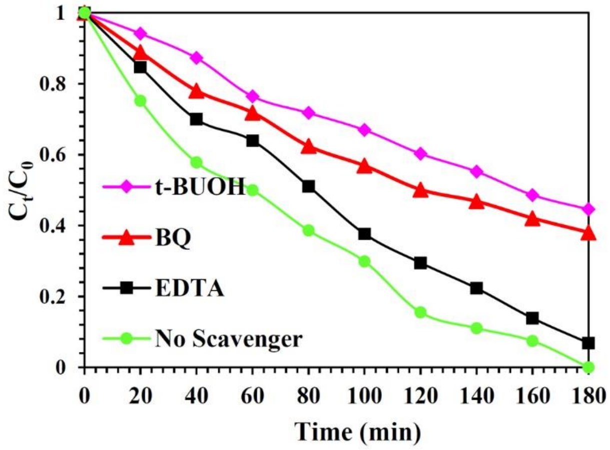

Fig. 7. Photocatalytic performance of WO_3-CeO_2 sample for degradation of Nitenpyram insecticide under visible light irradiation in presence of different scavengers.

and WO_3 samples are calculated around -0.54 and +0.8 eV vs. NHE, respectively. Further, E_V of CeO_2 and WO_3 samples are estimated through the equation $E_V=E_g + E_C$, therefore E_V of these samples are 2.16 and 3.4 eV vs. NHE, respectively.

Photocatalytic performance

The photocatalytic efficiencies of the prepared photocatalyst samples were examined by measuring the degradation of Nitenpyram insecticide under visible light irradiation. As shown in Fig. 6a, in the absence of any photocatalyst sample (Blank) the degradation of Nitenpyram is negligible while in the presence of CeO_2, WO_3 and their nanocomposite samples, an impressive degradation of Nitenpyram is occurred. The WO_3-CeO_2 heterojunction photocatalysts have the significantly improved photocatalytic performances than the pure CeO_2, WO_3 samples, which can be attributed to the decreasing of the charge carriers recombination rate and improvement of the visible light absorbance harvesting. Among the various WO_3-CeO_2 heterojunction nanocomposites, the sample with 30 wt% CeO_2 content has the best photocatalytic activity. The apparent reaction rate constants (k_{app}) for degradation of Nitenpyram insecticide on the prepared samples were estimated from the Pseudo first-order reaction kinetic equation (Eq. (2)) based on the Langmuir-Hinshelwood model at low concentration of a pollutant (in this case Nitenpyram) [42].

$$\ln\left(\frac{C_0}{C_t}\right) = k_{app}t \quad \text{Eq.(2)}$$

Where C_0 and C_0 are concentrations of Nitenpyram at irradiation time (t) of 0 and t respectively. Fig. 6b provides Pseudo first-order reaction kinetic curves for photocatalytic degradation of Nitenpyram over the prepared photocatalysts. k_{app} of the CeO_2, WO_3, WO_3-10CeO_2, WO_3-20CeO_2, WO_3-30CeO_2, and WO_3-40CeO_2 samples are calculated as 0.003, 0.004, 0.005, 0.008, 0.017, and 0.012 min^{-1}, respectively. Therefore, presence of CeO_2 in the structure of WO_3 at optimum weight percentage of 30 wt% could improve its photocatalytic activity about 4 times. Although, there are some reports about photocatalytic degradation of Nitenpyram [43-45], however, in the current work we introduced a new photocatalyst for this purpose, which because of the innovative hydrothermal preparation method by using tragacanth mucilage as natural surfactant and good distribution of CeO_2 and WO_3 semiconductors in each other's this heterojunction nanocomposite has improved photocatalytic performance under visible light irradiation.

To further investigate the role of the active species during the photocatalytic decomposition of Nitenpyram insecticide on the WO_3-CeO_2 heterojunction, tert-Butyl alcohol (t-BUOH) as $OH^{\bullet}$ scavenger, benzoquinone (BQ) as $O_2^{\bullet-}$ scavenger, and Ethylenediaminetetraacetic acid (EDTA) as hole scavenger [46], were added to the photocatalytic reaction suspension. Fig. 7 clearly indicates the highest decreasing of the photocatalytic performance in presence of t-BUOH, which distinctly demonstrates the dominant role of $OH^{\bullet}$ radicals in photocatalytic

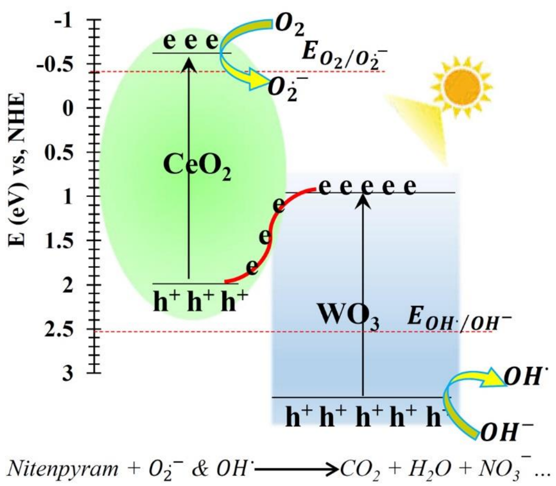

Fig. 8. Plausible S-scheme charge transfer pathways for the photocatalytic activity of the WO_3-CeO_2 heterojunction.

degradation of Nitenpyram insecticide. Moreover, the photocatalytic activity is also decreased in presence of BQ. In brief, the $OH^{\bullet}$ is the major cause of the photocatalytic degradation of Nitenpyram over the WO_3-CeO_2 nanocomposite under visible light irradiation, moreover, $O_2^{\bullet-}$ radicals are also involved during the degradation reactions.

Proposed mechanism of degradation

Plausible S-scheme charge transfer pathways for the photocatalytic activity of the WO_3-CeO_2 heterojunction are thoroughly discussed in Fig. 8. In this mechanism, during the irradiation of the heterojunction photocatalyst, the electrons on conduction band of WO_3 migrate to the valance band of CeO_2 [47]. In this regard, the charge carriers are efficiently separated, and produce the more $O_2^{\bullet-}$ and $OH^{\bullet}$ radicals. In this mechanism, the oxidation power of the photoinduced electrons and holes is improved, which results in the enhancement of the photocatalytic activity.

CONCLUSION

In summary, a novel S-scheme heterojunction photocatalyst was fabricated through a simple hydrothermal method from CeO_2 nanoparticles and WO_3 nanoplates in presence of tragacanth mucilage as natural surfactant, and was applied for first time for photocatalytic degradation of Nitenpyram insecticide under visible light irradiation. According to the XRD and SEM results, the WO_3-CeO_2 heterojunction has good crystallinity and contains CeO_2 nanoparticles and WO_3 nanoplates with good dispersedly. Moreover, the highest photocatalytic efficiency with rate constant of 0.017 min^{-1}, was obtained for the heterojunction sample with 30 wt% CeO_2 content which can be attributed to the decreasing of the charge carrier's recombination rate, and enhanced visible light harvesting. Moreover, based on the radical trapping experiments and Mott-Schottky calculations, hydroxide radical was determined as the main active species for degradation of Nitenpyram insecticide, and a S-scheme charge transfer mechanism revealed to be responsible for the enhanced photocatalytic performance.

FUNDING

There is no funding source for this work.

DECLARATION OF INTEREST AND VERIFICATION

The authors declare that they have no known competing financial interests or personal relationships that could have appeared to influence the results reported in this work.

REFERENCES

1. DiBartolomeis M., Kegley S., Mineau P., Radford R., Klein K., (2019), An assessment of acute insecticide toxicity loading (AITL) of chemical pesticides used on agricultural land in the United States. *PloS One*. 14: e0220029.
2. Liu J., Xiong W. H., Ye L. Y., Zhang W. S.,Yang H., (2020), Developing a novel nanoscale porphyrinic metal–organic framework: A bifunctional platform with sensitive fluorescent detection and elimination of nitenpyram in agricultural environment. *J. Agricult. food Chem.* 68: 5572-5578.
3. Priya R., Ramesh D., Khosla E., (2020), Biodegradation of pesticides using density-based clustering on cotton crop

affected by Xanthomonas malvacearum. *Environ. Develop. Sustainab.* 22: 1353-1369.
4. Dumée L. F., Maina J. W., Merenda A., Reis R., He L.,Kong L., (2017), Hybrid thin film nano-composite membrane reactors for simultaneous separation and degradation of pesticides. *J. Memb. Sci.* 528: 217-224.
5. Narayanan N., Gupta S.,Gajbhiye V. T., (2020), Decontamination of pesticide industrial effluent by adsorption–coagulation–flocculation process using biopolymer-nanoorganoclay composite. *Int. J. Environm. Sci. Technol.* 17: 4775-4786.
6. Wang R., Pan J., Qin M.,Guo T., (2019), Molecularly imprinted nanocapsule mimicking phosphotriesterase for the catalytic hydrolysis of organophosphorus pesticides. *Europ. Polym. J.* 110: 1-8.
7. Bhat A. P., Gogate P. R., (2021), Degradation of nitrogen-containing hazardous compounds using advanced oxidation processes: A review on aliphatic and aromatic amines, dyes, and pesticides. *J. Hazard. Mater.* 403: 123657.
8. Akerdi A. G., Bahrami S. H., (2019), Application of heterogeneous nano-semiconductors for photocatalytic advanced oxidation of organic compounds: A review. *J. Environm. Chem. Eng.* 7: 103283.
9. Azari B., Pourahmad A., Sadeghi B., Mokhtary M., (2020), Incorporation of Zinc Oxide nanoparticles in RHA-MTW zeolite and its application for degradation of dye. *J. Nanoanalysis*. 7: 179-189.
10. Dutta V., Sharma S., Raizada P., Thakur V. K., Khan A. A. P., Saini V., Asiri A. M., Singh P., (2021), An overview on WO_3 based photocatalyst for environmental remediation. *J. Environm. Chem. Eng.* 9: 105018.
11. Murillo-Sierra J., Hernández-Ramírez A., Hinojosa-Reyes L., Guzmán-Mar J., (2021), A review on the development of visible light-responsive WO_3-based photocatalysts for environmental applications. *Chem. Eng. J. Adv.* 5: 100070.
12. Zhang X., Wei Y.,Yu R., (2022), Multidimensional tungsten oxides for efficient solar energy conversion. *Small Struct.* 3: 2100130.
13. Mim R. S., Aldeen E. S., Alhebshi A., Tahir M., (2021), Recent advancements in strategies to improve performance of tungsten-based semiconductors for photocatalytic hydrogen production: A review. *J. Phys. D: Appl. Phys.* 54: 36-42.
14. Yang G., Zhu X., Cheng G., Chen R., Xiong J., Li W.,Wei Y., (2021), Engineered tungsten oxide-based photocatalysts for CO_2 reduction: Categories and roles. *J. Mater. Chem. A*. 9: 22781-22809.
15. Samuel O., Othman M. H. D., Kamaludin R., Sinsamphanh O., Abdullah H., Puteh M. H., Kurniawan T. A., (2021), WO_3–based photocatalysts: A review on synthesis, performance enhancement and photocatalytic memory for environmental applications. *Ceram. Int.* 48: 5845-5875.
16. Liao M., Su L., Deng Y., Xiong S., Tang R., Wu Z., Ding C., Yang L.,Gong D., (2021), Strategies to improve WO_3-based photocatalysts for wastewater treatment: A review. *J. Mater. Sci.* 56: 14416-14447.
17. Wang F., Di Valentin C.,Pacchioni G., (2012), Doping of WO_3 for photocatalytic water splitting: hints from density functional theory. *J. Phys. Chem. C.* 116: 8901-8909.
18. Fakhri H., Bagheri H., (2020), Highly efficient Zr-MOF@WO_3/graphene oxide photocatalyst: Synthesis, characterization and photodegradation of tetracycline and malathion. *Mater. Sci. Semicond. Process*. 107: 104815-104819.
19. Manikandan V., Harish S., Archana J., Navaneethan M., (2022), Fabrication of novel hybrid Z-Scheme WO_3@g-C_3N_4@MWCNT nanostructure for photocatalytic degradation of tetracycline and the evaluation of antimicrobial activity. *Chemosphere*. 287: 132050-132056.
20. Farhadian M., Sangpour P., Hosseinzadeh G., (2015), Morphology dependent photocatalytic activity of WO_3 nanostructures. *J. Energy Chem*. 24: 171-177.
21. Zhao T., Qian R., Zhou G., Wang Y., Lee W. I., Pan J. H., (2021), Mesoporous WO_3/TiO_2 spheres with tailored surface properties for concurrent solar photocatalysis and membrane filtration. *Chemosphere*. 263: 128344-128349.
22. He L., Zhang S., Zhang J., Chen G., Meng S., Fan Y., Zheng X., Chen S., (2020), Investigation on the mechanism and inner impetus of photogenerated charge transfer in WO_3/ZnO heterojunction photocatalysts. *J. Phys. Chem. C*. 124: 27916-27929.
23. Yang H., (2021), A short review on heterojunction photocatalysts: Carrier transfer behavior and photocatalytic mechanisms. *Mater. Res. Bullet.* 142: 111406-111411.
24. Bahadoran A., Farhadian M., Hoseinzadeh G., Liu Q., (2021), Novel flake-like Z-Scheme Bi_2WO_6-$ZnBi_2O_4$ heterostructure prepared by sonochemical assisted hydrothermal procedures with enhanced visible-light photocatalytic activity. *J. Alloys and Comp.* 883: 160895-160901.
25. Behara D. K., Priya Alugoti D. V., Sree P. P., (2020), Multi element doped type-II heterostructure assemblies (N, S-TiO_2/ZnO) for electrochemical crystal violet dye degradation. *Int. J. Nano Dimens.* 11: 303-311.
26. Azari B., Pourahmad A., Sadeghi B., Mokhtary M., (2019), Preparation and photocatalytic study of SiO_2/CuS coreshell nanomaterial for degradation of methylene blue dye. *Nanoscale*. 6: 103-114.
27. Prajapati P. K., Malik A., Nandal N., Pandita S., Singh R., Bhandari S., Saran S., Jain S. L., (2022), Morphology controlled Fe and Ni-doped CeO_2 nanorods as an excellent heterojunction photocatalyst for CO_2 reduction. *Appl. Surf. Sci.* 588: 152912-152918.
28. Ye K., Li Y., Yang H., Li M., Huang Y., Zhang S., Ji H., (2019), An ultrathin carbon layer activated CeO_2 heterojunction nanorods for photocatalytic degradation of organic pollutants. *Appl. Catal. B: Environm.* 259: 118085-118091.
29. Xu B., Yang H., Zhang Q., Yuan S., Xie A., Zhang M., Ohno T., (2020), Design and synthesis of Sm, Y, La and Nd-doped CeO_2 with a broom-like hierarchical structure: A photocatalyst with enhanced oxidation performance. *Chem. Cat. Chem*. 12: 2638-2646.
30. Zhu C., Wei X., Li W., Pu Y., Sun J., Tang K., Wan H., Ge C., Zou W., Dong L., (2020), Crystal-plane effects of CeO_2 {110} and CeO_2 {100} on photocatalytic CO_2 reduction: Synergistic interactions of oxygen defects and hydroxyl groups. *ACS Sustain. Chem. Eng.* 8: 14397-14406.
31. Nie J., Zhu G., Zhang W., Gao J., Zhong P., Xie X., Huang Y., Hojamberdiev M., (2021), Oxygen vacancy defects-boosted deep oxidation of NO by β-Bi_2O_3/CeO_2-δ pn heterojunction photocatalyst in situ synthesized from Bi/Ce(CO_3)(OH) precursor. *Chem. Eng. J.* 424: 130327-130331.
32. Hao C.-C., Tang Y.-B., Shi W.-L., Chen F.-Y., Guo F., (2021), Facile solvothermal synthesis of a Z-Scheme 0D/3D CeO_2/$ZnIn_2S_4$ heterojunction with enhanced photocatalytic performance under visible light irradiation. *Chem. Eng. J.* 409: 128168-128173.

33. Xiao Y., Ji Z., Zou C., Xu Y., Wang R., Wu J., Liu G., He P., Wang Q., Jia T., (2021), Construction of CeO_2/BiOI S-scheme heterojunction for photocatalytic removal of elemental mercury. *Appl. Surf. Sci.* 556: 149767-149771.
34. Zhao X., Guan J., Li J., Li X., Wang H., Huo P., Yan Y., (2021), CeO_2/3D g-C_3N_4 heterojunction deposited with Pt cocatalyst for enhanced photocatalytic CO_2 reduction. *Appl. Surf. Sci.* 537: 147891-147995.
35. Hu L., Zheng X., Zhu J., He J., (2022), Adsorption performance of CeO_2@NS-$HNbMoO_6$ for ethyl mercaptan in methane gas. *Chem. Papers.* 76: 2495-2504.
36. Chen J., Xiao X., Wang Y.,Ye Z., (2019), Fabrication of hierarchical sheet-on-sheet WO_3/g-C_3N_4 composites with enhanced photocatalytic activity. *J. Alloys Comp.* 777: 325-334.
37. Arya S., Chhina M. K., Choudhary R., Dua V., Singh K., (2022), Growth of different nanocrystalline phases in ZnO–Li_2O–B_2O_3–TiO_2–V_2O_5 glass and their effect on photoluminescence and photocatalytic activity. *Ceram. Int.* 48: 20619-20626.
38. Zinatloo-Ajabshir S., Emsaki M., Hosseinzadeh G., (2022), Innovative construction of a novel lanthanide cerate nanostructured photocatalyst for efficient treatment of contaminated water under sunlight. *J. Colloid Interf. Sci.* 619: 1-13.
39. Liqiang J., Yichun Q., Baiqi W., Shudan L., Baojiang J., Libin Y., Wei F., Honggang F., Jiazhong S., (2006), Review of photoluminescence performance of nano-sized semiconductor materials and its relationships with photocatalytic activity. *Solar Energy Mater. Solar Cells.* 90: 1773-1787.
40. Gelderman K., Lee L., Donne S., (2007), Flat-band potential of a semiconductor: Using the Mott–Schottky equation. *J. Chem. Educ.* 84: 685-692.
41. Hosseinzadeh G., Zinatloo-Ajabshir S., Yousefi A., (2022), Innovative synthesis of a novel ZnO/$ZnBi_2O_4$/graphene ternary heterojunction nanocomposite photocatalyst in the presence of tragacanth mucilage as natural surfactant. *Ceram. Int.* 48: 6078-6086.
42. Akhlaghian F., Najafi A., (2018), CuO/WO_3/TiO_2 photocatalyst for degradation of phenol wastewater. *Scientia Iranica*. 25: 3345-3353.
43. Teye G. K., Huang J., Li Y., Li K., Chen L., Darkwah W. K., (2021), Photocatalytic degradation of sulfamethoxazole, nitenpyram and tetracycline by composites of core shell g-C_3N_4@ZnO, and ZnO Defects in aqueous phase. *Nanomater.* 11: 2609-2615.
44. Zhou S., Wang Y., Zhou K., Ba D., Ao Y., Wang P., (2021), In-situ construction of Z-scheme g-C_3N_4/WO_3 composite with enhanced visible-light responsive performance for nitenpyram degradation. *Chin. Chem. Lett.* 32: 2179-2182.
45. Pei Z., Wang C., Wang P., Zhou G., (2022), Covalent-anion-driven self-assembled cadmium/molybdenum sulfide hybrids for efficient nitenpyram degradation. *J. Environm. Manag.* 316: 115269-115274.
46. Khalid N., Ishtiaq H., Ali F., Tahir M., Naeem S., Ul-Hamid A., Ikram M., Iqbal T., Kamal M. R., Alrobei H., (2022), Synergistic effects of Bi and N doped on ZnO nanorods for efficient photocatalysis. *Mater. Chem. Phys.* 289: 126423-126429.
47. Xu Q., Zhang L., Cheng B., Fan J., Yu J., (2020), S-scheme heterojunction photocatalyst. *Chem*. 6: 1543-1559.